Mon. Not. R. Astron. Soc. **000**, 1–10 (2002) Printed 2 February 2008 (MN LATEX style file v2.2)

The X-ray/γ-ray spectrum of XTE J1550–564 in the very high state

Marek Gierliński[1,2] and Chris Done[1]
[1]*Department of Physics, University of Durham, South Road, Durham DH1 3LE, UK*
[2]*Obserwatorium Astronomiczne Uniwersytetu Jagiellońskiego, 30-244 Kraków, Orla 171, Poland*

arXiv:astro-ph/0212384v2 12 Mar 2003

Submitted to MNRAS

ABSTRACT

We fit the broad-band X/γ-ray spectrum (0.8–1000 keV) of the accreting black hole XTE J1550–564 in the very high state. The quasi-simultaneous data from *ASCA*, *RXTE* and OSSE show that the disc is strongly Comptonized, with a high energy tail extending out to several hundreds keV. However, inverse Compton scattering by a purely thermal or purely power-law electron distribution cannot explain the observed spectrum. Instead the data require a hybrid distribution, with both thermal and non-thermal electrons scattering the disc photons. This is very similar to the electron distribution inferred for other high and very high state black hole binaries, showing that it is a generic feature of high mass accretion rate black holes.

Key words: accretion, accretion discs – X-rays: individual: XTE J1550–564 – X-rays: binaries – radiation mechanisms: non-thermal

1 INTRODUCTION

Galactic black hole candidates show variety of spectra at X-ray and γ-ray energies. These can be roughly described in terms of a soft, quasi-thermal component from the accretion disc together with a power-law-like tail extending to much higher energies. Five 'canonical' spectral states have been identified historically, based on the luminosity and spectral shape (see e.g. Esin, McClintock & Narayan 1997 and references therein). The *very high state* is generally seen at the highest luminosities, where the soft thermal component (with temperature of 0.5–1 keV) and power-law tail (photon spectral index Γ = 2–3) have comparable power. In the *high state* the hard tail is much weaker or sometimes even not present. The *intermediate state* is rather like the very high state, but at lower disc temperature and luminosity (Belloni et al. 1996; Méndez & van der Klis 1997), while the *low state* is somewhat different, being characterised by a hard ($\Gamma < 2$) power-law-like spectrum with a very weak, low temperature disc component (Bałucińska-Church et al. 1995; di Salvo et al. 2001). At very low luminosities, transient sources go into the *quiescent state*, which is a very low luminosity version of the *low state* (Kong et al. 2000; Sutaria et al. 2002). The high and very high states are often described as soft states, while the low state is commonly referred to as a hard state. Persistent sources like Cyg X-1 and LMC X-1 spend most of their time in one state, however transients like Nova Muscae can progress through a sequence of all five states during an outburst (Ebisawa et al. 1994). See Done & Gierliński (2003) for an overview of these spectral states.

The power-law-like tails extending to X/γ-ray energies are commonly explained by Compton up-scattering of the soft seed photons from the accretion disc by a population of high-energy electrons. In the low/hard state the observed hard spectra roll over at 100–200 keV, indicating that the electrons are mostly thermal (with typical temperatures of $\sim$ 100 keV) and have optical depth of order unity (e.g. Gierliński et al. 1997; Zdziarski et al. 1998; Frontera et al. 2001). By contrast, in the soft states the steeper tail extends unbroken to MeV energies (Grove et al. 1998), indicating that the electron energy distribution is predominantly non-thermal. More detailed spectral studies of the very high- and high-state spectra show that the tail is best described by Comptonization from a complex electron distribution, where there is both a low temperature ($\sim$ 10 keV) thermal electron distribution (Życki, Done & Smith 2001; Kubota, Makishima & Ebisawa 2001) together with non-thermal power-law electrons (Gierliński et al. 1999; Zdziarski et al. 2002). A two-component electron distribution could arise fairly naturally from non-thermal electron acceleration regions powered by magnetic reconnections above a disc. Low-energy electrons cool preferentially by Coulomb collisions leading to a thermal distribution while the high-energy electrons cool by Compton scattering, preserving a non-thermal distribution (Coppi 1999). Alternatively, the thermal and non-thermal electrons could be spatially distinct, e.g. magnetic reconnection above the disc can produce a non-thermal electron distribution, while overheating of the inner disc produces the thermal Comptonization (Kubota et al. 2001).

The soft and hard states are clearly distinct in their spectral properties (e.g. Zdziarski et al. 2002). Transition between the states is compatible with being driven by a changing accretion geometry, where the low state has an accretion disc only at large radii, with the inner disc being replaced by a hot, optically thin, geometrically thick flow (e.g. Poutanen, Krolik & Ryde 1997). With increasing accretion rate the disc moves inwards increasing its temperature and the number of seed photons cooling the inner flow so the Comptonized spectrum becomes softer. Eventually, when the inner flow becomes optically thick it collapses, the inner disc re-

© 2002 RAS

places the hot flow and the source reaches one of the soft states (see e.g. Esin et al. 1997).

This review of spectral properties draws heavily from the very few broad bandpass X/γ-ray observations of black holes. To constrain both the disc and hard component requires simultaneous data over a broad energy range, ideally $\sim$ 0.1–1000 keV. While both the Phoswich Detector System on board *BeppoSAX* and High Energy X-ray Timing Experiment (HEXTE) on board *Rossi X-ray Timing Explorer* (*RXTE*) can give data out to $\sim$ 100–200 keV, the Oriented Scintillation Spectrometer Experiment (OSSE) on the *Compton Gamma Ray Observatory* (*CGRO*) is unique in being able to extend the bandpass to higher energies. This is especially important in soft states, as there the hard component is known to extend to the highest energies. However, there are only very few broad-band observations of black hole candidates in these spectral states: GRS 1915+105 (Zdziarski et al. 2001; Ueda et al. 2002), GRO J1655–40 (Tomsick et al. 1999), Cyg X-1 (Gierliński et al. 1999; McConnell et al. 2002). However, both GRO J1655–40 and GRS 1915+105 are thought to be extreme Kerr black holes due to their high accretion disc temperatures (e.g. Zhang, Cui & Chen 1997), so there are *no* very high state broad-band spectra of 'normal' black holes.

In this paper we remedy the situation by analysing the broad-band simultaneous *RXTE*/OSSE data of the X-ray black hole transient XTE J1550–564, and derive constraints on the electron distribution and accretion flow geometry. We show that the hard tail is remarkably similar to that seen in the extreme Kerr, microquasar black holes, so it is most probably a generic feature of high mass accretion rate flow onto a black hole rather than being associated with spin or radio jets.

2 THE SOURCE

The X-ray nova XTE J1550–564 was discovered during its spectacular outburst in 1998 (Smith et al. 1998). Two weeks into the outburst it reached a peak flux of 6.8 crab (1.6×10^{-7} erg s^{-1} cm^{-2}) in 2–10 keV energy range, making it the brightest X-ray transient observed so far by *RXTE*. The X-ray (2–10 keV) lightcurve from All-Sky Monitor (ASM), is more complex than a fast rise, exponential decay, having a bright flare followed by two plateaus separated by a weak minimum. Such lightcurves are not uncommon (see e.g. Chen, Shrader & Livio 1997), and are probably connected to enhanced mass transfer from the irradiated companion star (Esin, Lasota & Hynes 2000). The complex X-ray spectral evolution during the outburst is shown in Fig. 1 by comparing the 2–10 keV lightcurve from ASM to the harder X-ray (20–100 keV) lightcurve from *CGRO* Burst And Transient Source Experiment (BATSE). More details of this spectral evolution are given in Sobczak et al. (2000), Homan et al. (2001), Wilson & Done (2001) and Kubota et al. (2003).

Observations of the optical companion (Orosz et al. 2002) led to an estimate of the compact object mass, 8.4–10.8 M$_\odot$, confirming its black hole nature. The inclination angle of the binary is quite high, 67°–77.4° (both estimates are given with 1σ errors, the 3σ ranges are 6.8–15.6 M$_\odot$ and 55°–79°, respectively). The distance is less well constrained by their data on the optical companion, with D = 3.0–7.6 kpc (best fit value of 5.3 kpc). Throughout this paper we assume M = 10M$_\odot$, $i = 70°$ and D = 5.3 kpc.

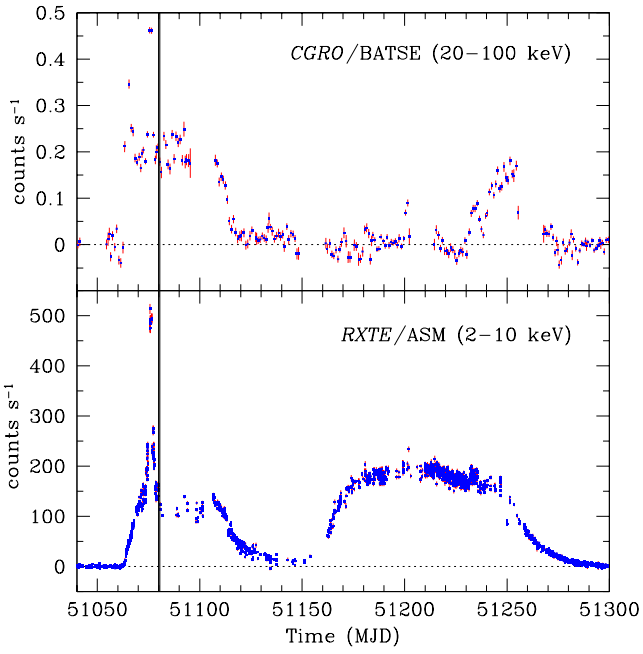

Figure 1. BATSE and ASM lightcurves of 1998 outburst of XTE J1550–564. Vertical line marks the OSSE viewing period 729.5, analysed in this paper together with simultaneous *RXTE* observations. The *ASCA* observations was made one day before the OSSE viewing period 729.5 had started.

3 THE DATA

In this paper we analyse the contemporaneous X/γ-ray spectra of XTE J1550–564 from *ASCA*, *RXTE* and OSSE in a period from 1998 September 23 to 1998 October 6 (MJD 51080–51092) i.e. in the first part of the outburst, in the plateau just after the strong flare. There are *RXTE* observations over this entire period, while the *ASCA* data are limited to a snapshot at the start (September 23/24) which does not quite overlap with the *OSSE* data (between September 25 and October 6). The times of our data are shown on the soft and hard X-ray lightcurves of the outburst in Fig. 1 while a detailed observation log is presented in Table 1.

We used the standard product *ASCA* Gas Imaging Spectrometer (GIS) spectrum from detector 2, with response matrix version 4.0, corrected for dead time (Makishima et al. 1996). Since the source is very bright we fit the GIS2 spectrum alone to avoid possible cross-calibration uncertainties between GIS2 and GIS3. There is a simultaneous *RXTE* pointing (observation number 30191-01-10-00), but we treat the *ASCA* data separately to avoid the significant cross-calibration issues between *RXTE* and *ASCA* (e.g. Done, Madejski, Życki 2000).

The *OSSE* data for viewing period 729.5 extends between September 25 and October 6 (Fig. 1). We use a high-level product spectrum extracted for detectors 1, 2, 3 and 4, for the whole viewing period. Due to rather large OSSE field of view ($11° \times 3.8°$; Johnson et al. 1993) there is always a danger of a background source contaminating the spectrum. Therefore, we compare the OSSE spectrum with the simultaneous HEXTE spectrum. Since HEXTE has much smaller field of view ($\sim 1°$; Rothschild et al. 1998), contamination by a background source is much less probable. The excellent agreement between the HEXTE and OSSE spectra (see Section 5.2) make contamination by a background source rather unlikely.

RXTE observed the source 15 times during OSSE viewing period 729.5, with observation archival numbers (obsids) between

Table 1. Log of observations.

Instrument	Detectors	Observation ID	Time (MJD)	Live time (s)	Count rate (cnt s^{-1})
ASCA GIS	2	15606010	51079.964–51080.500	25156	93.30±0.06
RXTE PCA	01, layer 1	30191-01-12-00 ... -23-00	51082.003–51091.790	45664	5891±6
RXTE HEXTE	0	30191-01-12-00 ... -23-00	51082.003–51091.790	14442	287.8±0.2
CGRO OSSE	1234	729.5	51081.640–51092.561	496313	12.2±0.2

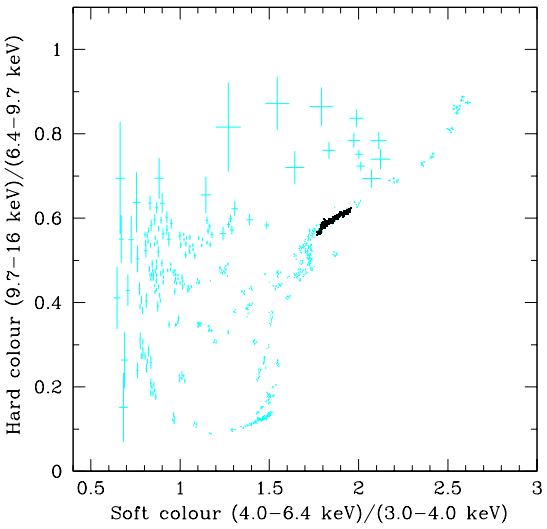

Figure 2. *RXTE*/PCA colour-colour diagram of the 1998 outburst of XTE J1550–564. The colours were corrected for the PCA gain changes (by the same method as in Gierliński & Done 2002) and rebinned for clarity. Data points in black denote the *RXTE* observations simultaneous with OSSE viewing period 729.5.

30191-01-12-00 and 30191-01-23-00. To assess the source X-ray variability over this 10 day period we create a PCA colour-colour diagram, using a method described by Gierliński & Done (2002). The diagram, shown in Fig. 2, contains all the PCA data collected during the 1998/1999 outburst, and observations simultaneous with OSSE are marked in black. There is a shift in colours during this period, though it is small compared to the spectral variation seen during the whole outburst. This particular part of the colour-colour diagram corresponds to the very high spectral state (Done & Gierliński 2003).

We extract the PCA and HEXTE spectra using FTOOLS 5.2 for each of the aforementioned obsids, and also create a single spectrum for each instrument averaged over the whole OSSE viewing period. For the PCA, we extract the spectra from detectors 0 and 1, top layer only (see Wilson & Done 2001), correcting for the photon pile-up (Tomsick et al. 1999). For HEXTE we extract spectra from cluster 0 only.

4 SPECTRAL MODELS

As outlined in the introduction, the X-ray spectrum is probably formed by Compton scattering of the accretion disc seed photons. While an exponentially cutoff power law is often used as an approximation to a thermally Comptonized spectrum, this becomes very inaccurate if the observed bandpass approaches the typical seed photon or electron energies (e.g. Done, Życki & Smith 2002; Zdziarski et al. 1998). Since we have an extremely broad bandpass we use instead the best available Comptonization models, which properly calculate the shape of the high-energy rollover for thermal electrons, and include the low-energy cutoff close to the seed photon energies. There are currently two of these Comptonization codes available for spectral fitting, COMPPS (Poutanen & Svensson 1996) and EQPAIR (Coppi 1999). Both of these can calculate the spectra from thermal as well as non-thermal Comptonization.

The COMPPS code computes Comptonization in various specific geometries (we assume spherical) from a given electron distribution of total optical depth τ. This is split between a thermal distribution (Maxwellian, with temperature T_e) which is truncated at some Lorentz factor $\gamma_{\rm min}$, above which it has a non-thermal [power law, $N(\gamma) \propto \gamma^{-p}$] distribution up to Lorentz factor $\gamma_{\rm max}$.

The EQPAIR code is rather different in that it computes the electron distribution self-consistently, assuming that the electrons are injected with a power-law distribution of index $\Gamma_{\rm inj}$. The rate of Compton cooling is larger at higher energies, so the equilibrium distribution is softer than the injected one with index $p = \Gamma_{\rm inj} + 1$ (e.g. Blumenthal & Gould 1970). The electrons can also thermalize through Coulomb collisions, producing a hybrid, thermal/non-thermal distribution. However, the code also allows some fraction of the total power to be used to heat the thermal distribution directly. The microscopic processes are calculated in the plasma cloud of assumed optical depth of ionization electrons, $\tau_{\rm ion}$. The total optical depth, $\tau = \tau_{\rm ion} + \tau_{\rm pair}$, is calculated self-consistently, including the additional optical depth in electron-positron pairs, $\tau_{\rm pair}$, produced by photon-photon collisions. The plasma properties depend on its compactness

$$\ell \equiv \frac{\sigma_{\rm T}}{m_{\rm e}c^3}\frac{\mathcal{L}}{\mathcal{R}}, \qquad (1)$$

where $\mathcal{L}$ is the power supplied to the plasma, $\mathcal{R}$ is its characteristic size, $\sigma_{\rm T}$ is the Thompson cross section and m_e is the electron mass. The power supplied to the electrons is parameterized as a hard compactness, $\ell_{\rm h}$, while the power in soft seed photons is given as a soft compactness, $\ell_{\rm s}$. The hard compactness is split into non-thermal electron acceleration and direct thermal heating, denoted $\ell_{\rm nth}$ and $\ell_{\rm th}$, respectively, where $\ell_{\rm h} = \ell_{\rm nth} + \ell_{\rm th}$. The electron temperature, T_e, is calculated self-consistently from the balance between cooling and heating. We note that even when the whole power is supplied to non-thermal electrons (i.e. $\ell_{\rm th} = 0$), the Coulomb cooling can dominate at lower energies over Compton cooling, so the electrons will form a hybrid distribution. The model parameters are $\ell_{\rm s}$, $\ell_{\rm h}/\ell_{\rm s}$, $\ell_{\rm nth}/\ell_{\rm h}$, $\Gamma_{\rm inj}$ and $\tau_{\rm ion}$.

Both models include the reflected continuum computed from the incident continuum using the Green's functions of Magdziarz & Zdziarski (1995). This is relativistically smeared (Fabian et al. 1989), but does not include the self-consistently produced iron Kα line, so we include this separately using the DISKLINE model (Fabian et al. 1989), with relativistic smearing set equal to that of the reflected continuum. These are parameterized by the solid angle of the reflecting medium, Ω, its ionization, ξ, and the inner disc

radius, $R_{\rm ref}$. The rest-frame energy of the line is denoted as $E_{\rm line}$ and its equivalent width as EW.

For purely thermal Comptonization we also use a more approximate (but faster) THCOMP code (Zdziarski, Johnson & Magdziarz 1996), which is based on Kompaneets (1956) equation. This assumes that the photons diffuse in both time and space (Sunyaev & Titarchuk 1980), which becomes inaccurate for temperatures above ~ 50 keV, as such photons lose a large fraction of their energy in Compton down-scattering.

In all of these models we assume that the seed photons for Comptonization have a multi-colour disc blackbody (model DISKBB; Mitsuda et al. 1984) distribution, with temperature $T_{\rm seed} = T_{\rm diskbb}$. We allow for additional disc photons which do not pass through the Comptonizing region, e.g. corresponding to a fraction of the disc not covered by a patchy corona. For calculating inner disc radius we take into account all disc photons, both seed and non-seed. In figures we plot only the disc photons which reach the observer unscattered.

5 RESULTS

For spectral fitting we use the X-ray spectral fitting package XSPEC version 11 (Arnaud 1996), with our own implementation of the Comptonization models described above. The error of each model parameter is given for a 90 per cent confidence interval ($\Delta\chi^2 = 2.7$). We use the 0.9–10 keV GIS data, 3–20 keV PCA data, 20–150 keV HEXTE data and 50–1000 keV OSSE data. The relative normalizations of the PCA, HEXTE and OSSE are uncertain, so we allow them to be free parameters in simultaneous spectral fits. We base fluxes on the PCA normalization.

5.1 *ASCA*

The near-simultaneous *ASCA* observation gives us an excellent opportunity to study the soft X-ray part of the XTE J1550–564 spectrum, not covered by *RXTE* and OSSE. From the PCA data we know that the X-ray spectrum did not change much between *ASCA* and OSSE observations, so we can apply the seed photon temperature, $T_{\rm seed}$, and Galactic absorption, N_H, obtained from *ASCA* to the *RXTE*/OSSE spectral fits.

We use all three Comptonization models to check that the results do not depend on the details of the models used. The *ASCA* data are not sensitive to the details of the high energy spectrum, so we assume that the Comptonizing electrons are thermal with electron temperature fixed at kT_e = 30 keV (COMPPS and THCOMP) or equivalently $\tau_{\rm ion} = 2$ for EQPAIR.

Our model consists of this thermal Comptonization (together with its reflected continuum and associated iron line emission), and a multicolour disc blackbody. All three models for the Comptonized continuum give almost identical values of N_H and $T_{\rm seed}$ (Table 2). We check that our choice of T_e (or equivalently $\tau_{\rm ion}$) did not affect these values, and even replacing the disc spectrum by a single-temperature blackbody gives only a slightly lower column of about 6.0×10^{21} cm^{-2}.

This result is not very different from previous findings. Jain et al. (1999) found $N_H \approx 9 \times 10^{21}$ cm^{-2} from optical reddening in the direction of XTE J1550–564. Kong et al. (2002) fit the *Chandra* spectra of XTE J1550–564 in quiescence with various models and found N_H between 3 (blackbody) and 9×10^{21} cm^{-2} (power law). Thought it not clear what spectral shape should we expect from a black hole binary in a quiescence, Tomsick, Corbel & Kaaret (2001) point out that the blackbody model leads to rather unphysical size of the source, ~ 0.1 km. Raymond-Smith, bremsstrahlung and power law models with *Chandra* data all give N_H consistent with our result. We note that a much larger column of 2×10^{22} cm^{-2} found by Sobczak et al. (2000) from the PCA fits is due to lack of sensitivity of the PCA below ~ 3 keV. And indeed, when we allow N_H to be a free parameter in our *RXTE*/OSSE fit (see below, Section 5.3), it yields $N_H \approx 2.5 \times 10^{22}$ cm^{-2}.

Table 2. Fits of a multicolour disc blackbody plus thermal Comptonization (and its associated reflection spectrum and iron line) to the *ASCA* spectrum. The seed photons for Comptonization are assumed to be from the disc, with $T_{\rm seed} = T_{\rm in}$.

Model	N_H (10^{21} cm^{-2})	$kT_{\rm diskbb}$ (keV)	χ^2/ν
THCOMP	$6.48^{+0.09}_{-0.10}$	$0.529^{+0.012}_{-0.012}$	209.0/184
COMPPS	$6.49^{+0.07}_{-0.12}$	$0.528^{+0.013}_{-0.011}$	206.7/184
EQPAIR	$6.53^{+0.10}_{-0.10}$	$0.531^{+0.012}_{-0.012}$	207.4/184

Strongly ionized reflection is significantly detected in all these models (see also Wilson & Done 2001), but rather surprisingly the amount of relativistic smearing is small. From all three models we find very high inner disc radius, typically $R_{\rm ref} > 200 R_g$ (where $R_g \equiv GM/c^2$ is the gravitational radius). However, closer investigation of the residuals shows that this is driven by narrow features in the spectrum around the iron line energy. A disc which extends much further into the gravitational potential is consistent with the data if there is a narrow absorption line at ~ 7.2 keV with 40 eV equivalent width. Such narrow features are seen from other X-ray binary systems viewed at high inclination, as GRO J1655–40 (Ueda et al. 1998) or GRS 1915+105 (Kotani et al. 2000), where it is interpreted as resonance absorption from iron, but the line energy we obtain in XTE J1550–564 is slightly too high. A P Cygni line profile, as seen in Cir X-1 (Brandt & Schulz 2000), gives an equally good fit to the XTE J1550–564 data, but with emission and absorption line energies (~ 6.9 and 7.0 keV, respectively) which are physically consistent with the resonant transition in Fe XXVI. However, the seed photon energy and absorption column are unchanged by these different models of the iron line structure. Thus the derived N_H and $T_{\rm seed}$ are fairly robust.

5.2 OSSE and HEXTE

The OSSE spectrum extracted from the entire viewing period give an excellent fit (χ^2/ν = 7.5/19) to a simple power law with photon spectral index $\Gamma = 3.09 \pm 0.04$. There is no evidence for any high-energy cutoff in the data with a lower limit on an exponential rollover energy of 990 keV.

The HEXTE data are evenly spread throughout the OSSE observation, so we can use the better signal to noise of the HEXTE instrument to look for spectral variability. The PCA data clearly shows that at lower energies there is indeed a small spectral change throughout this time, with root-mean-square variation in the soft and hard PCA colours of 2.9 and 2.6 per cent, respectively (Fig. 2). We fit the HEXTE spectrum from each *RXTE* obsid by a cutoff power law and Fig. 3 shows the resulting values of the e-folding energy, spectral index and flux. The spectral shape is consistent with remaining constant (with $\Gamma \sim 2.4$ and $E_c \sim 80$ keV) despite the 20–150 keV flux decreasing by ~ 15 per cent. Hence we are justified in co-adding all the HEXTE and OSSE data accumulated over this period to form a single spectrum from each instrument.

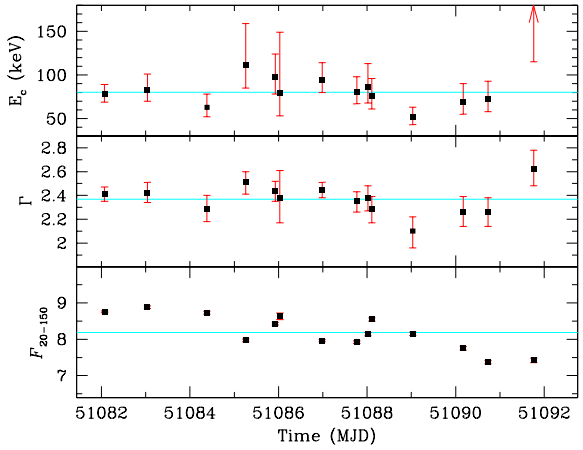

Figure 3. Variability of XTE J1550–564 in 20–150 keV range during OSSE observation. The HEXTE spectra were fitted by the cutoff power law and the panels show the e-folding energy, E_c, photon spectral index, Γ, and 20–150 keV model flux in 10^{-9} erg cm^{-2} s^{-1} units. Horizontal lines show average values of these parameters. The last observation for which only lower limit on E_c exists has been excluded from average of E_c.

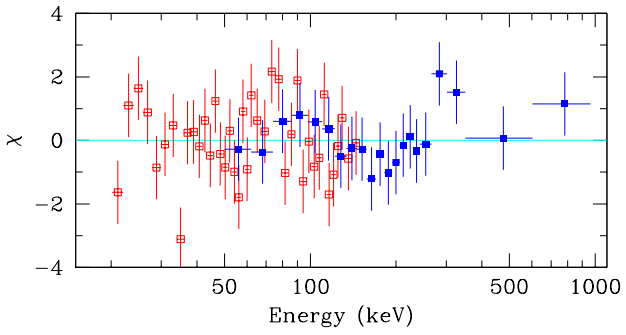

Figure 4. HEXTE and OSSE residuals. The data were fitted by a thermal Comptonization plus power law model. The relative normalization between HEXTE and OSSE was free.

Plainly, the power law and exponential cutoff models have very different parameters in the HEXTE and OSSE spectra, so a joint fit with this model gives a very poor χ^2. Fig. 4 shows the residuals of a joint fit of the two spectra to a phenomenological model of a power law plus thermal Comptonization model. The fit is reasonably good (χ^2/ν = 65.8/54), but more importantly, Fig. 4 clearly shows that the HEXTE and OSSE data are in very good agreement in their region of overlap. There are no big cross-calibration problems, or problems with a contaminating source in the large OSSE field of view.

5.3 *RXTE* and OSSE

Finally, we fit the averaged PCA, HEXTE and OSSE data together with the proper Comptonization models. We fix $N_H = 6.5 \times 10^{21}$ cm^{-2} and $kT_{\rm seed} = kT_{\rm diskbb} = 0.53$ keV from the *ASCA* results (Section 5.1). We estimate the inner radius from the DISKBB model, $R_{\rm diskbb}$, assuming distance of D = 5.3 kpc, inclination angle of $i = 70^\circ$. We correct it for spectral hardening due to scattering, assuming the ratio of colour to effective temperature of 1.8 (Shimura & Takahara 1995; Merloni, Fabian & Ross 2000). We also correct it for the inner torque-free boundary condition (Gierliński et al. 1999).

5.3.1 *Maxwellian and power-law electrons*

Purely thermal Comptonization (a model referred to as TH) cannot fit the observed spectrum. A model consisting of the disc blackbody, thermal Comptonization (any code described in Sec. 4) and its reflection/line gives $\chi^2/\nu \sim 5$. The best fit is shown in Fig. 5*a* and clearly shows that the spectral curvature in the lower energy data, which requires a fairly low temperature ($kT_e \sim 80$ keV, $\tau \sim 0.5$) thermal Compton component, is strongly inconsistent with the higher energy data. In principle, a very high electron temperature ($\gg 100$ keV) could fit the high-energy tail, but to have this together with a fairly steep overall spectrum requires a very low optical depth of the Comptonizing medium ($\tau < 0.1$). The spectrum from Comptonization in such an optically thin plasma consists of distinct humps from subsequent scattering orders, which are not present in the data. Moreover, the fraction of unscattered disc photons would be much larger than seen in the data.

The high-energy tail in the data can be reproduced in the model by adding a power law. This gives much better, though still statistically unacceptable fit (χ^2/ν = 161/93). This is because the high-energy data requires fairly hard power law ($\Gamma \approx 2.3$ from the fit) which extends down to lower energies and strongly contributes to the spectrum at soft X-rays, distorting it considerably.

Interestingly, a purely non-thermal, power-law electron distribution (model PL) cannot fit the data either ($\chi^2/\nu \sim 4$; Fig. 5*b*). This is because the spectrum from multiple Compton scatterings on power-law electrons is *not* a power law. The steep spectrum requires a soft electron index (best fit value of $p = 6.3$ from COMPPS). This means that the average electron energy is low, so photons must be scattered many times before they reach high energies (> 100 keV). In such multiple scatterings they reach the Klein-Nishina regime where the cross-section for the scattering decreases. This creates a break in the spectrum at a few hundred keV (Ghisellini 1989), so underpredicting the higher energy data above ~ 300 keV. Power-law electrons with very small optical depth would be able to produce an unbroken power-law photon spectrum on a single scattering. This, however, would give too large fraction of unscattered disc photons again.

Plainly, the data require a more complex continuum. Now we use a model PLTH, consisting of two Comptonizing regions (both computed with COMPPS): one with a Maxwellian (thermal) electron distribution, the other with power-law electrons. Both these Comptonize the seed photons from the disc independently. We obtain a very good fit with $\chi^2/\nu = 65.9/94$ (see Table 3). The spectrum at lower energies is dominated by the thermal component with temperature about 30 keV, while the high-energy tail is created by up-scattering seed photons on optically thin ($\tau \approx 0.3$), steep power-law ($p \approx 4.5$) electrons, where the break from the Klein-Nishina is masked by the thermal Compton component (Fig. 6*a*).

The requirement for both thermal and non-thermal electrons does not simply rest on the (rather weak) detection of the source at the highest energies in OSSE (3.7σ and 1.5σ for channels 350–600 keV and 600–900 keV, respectively). Instead it is driven by the overall spectral shape between ~ 100 and ~ 300 keV where the OSSE data have excellent statistics. Even the spectral fits with the OSSE data above 350 keV excluded strongly rule out purely thermal or purely power-law Comptonization models, as these both produce a much steeper high-energy cutoff than observed.

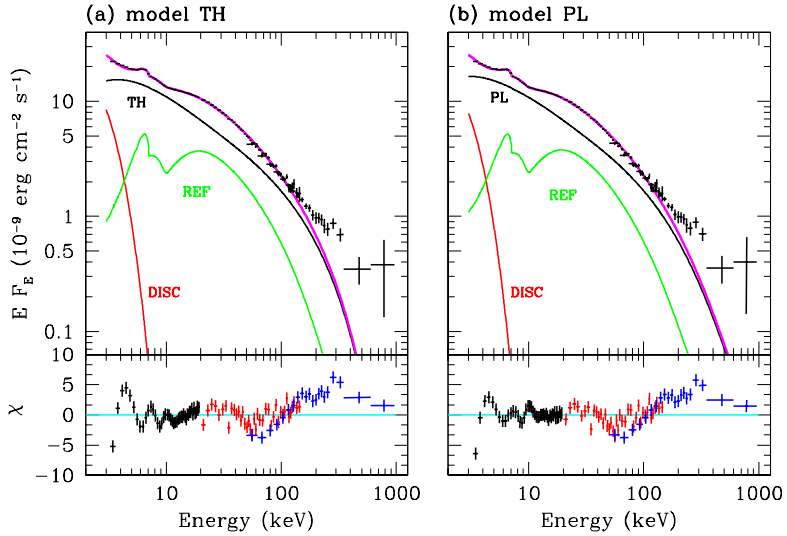

Figure 5. PCA, HEXTE and OSSE unfolded data, the best-fitting models and residuals. (a) Comptonization on Maxwellian electrons (TH). (b) Comptonization on power-law electrons (PL). Contribution from the multicolour blackbody disc (DISC) and Compton reflection (REF) are also shown.

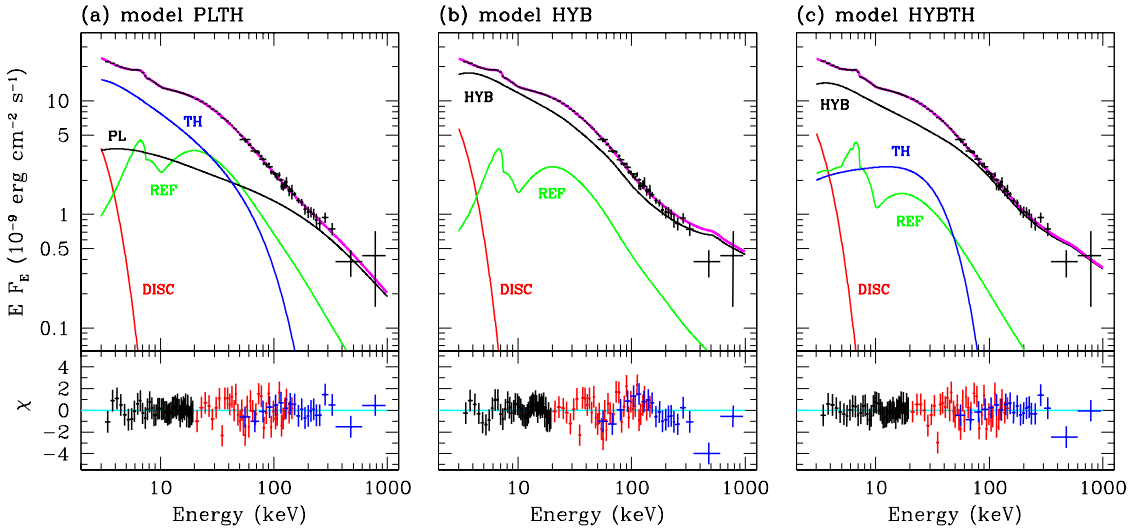

Figure 6. PCA, HEXTE and OSSE unfolded data, the best-fitting models and residuals. (a) with two Comptonizing regions: with power-law (PL) and thermal (TH) electrons. (b) Comptonization on hybrid (HYB) electron distribution. (c) hybrid electrons and additional thermal component. Contribution from the multicolour blackbody disc (DISC) and Compton reflection (REF) are also shown.

5.3.2 Hybrid electrons

Alternatively, the complex continuum could be produced by a single Comptonizing plasma, where non-thermal electrons partially thermalize through Coulomb collisions, creating a hybrid distribution: Maxwellian at lower energies and power-law at higher energies. We use EQPAIR to compute this distribution self-consistently, together with its reflection/line emission and seed photons from the disc (model HYB).

This hybrid model gives a somewhat worse fit ($\chi^2/\nu = 100.6/94$, see Table 4 and Fig. 6b) than the two Comptonizing regions model PLTH ($\chi^2/\nu = 63.4/92$), although it is still statistically an adequate description of the data. The reason the fit is different is that Comptonization from two separate electron distributions, where one is thermal and the other non-thermal, gives a subtly different spectrum to that of a single hybrid electron distribution. The sum of a thermal and power-law distribution has the power-law electrons also contributing to the spectrum at low energies, whereas in the hybrid electron distribution there are only the thermal electrons at low energies. While in principle this could give us a way to distinguish between the two models, in practice the situation is much less clear due to uncertainties in the reflected spectrum (see below).

Error ranges are hard to obtain as many of the parameters are correlated, so give multiple local minima in χ^2. In particular, the soft compactness, $\ell_{\rm s}$, is anti-correlated with the fraction of power in the non-thermal injection, $\ell_{\rm nth}/\ell_{\rm h}$. This is why in the model HYB we fixed $\ell_{\rm s}$ = 10. The soft compactness determines the strength of

Table 3. Fitting results of the model PLTH, consisting of two Comptonizations: on thermal (temperature $T_{\rm th}$ and optical depth $\tau_{\rm th}$) and power-law (index p and optical depth $\tau_{\rm pl}$) electrons. Values in parentheses refer to the parameters fixed during the fit. The unfolded data and model of this fit are shown in Fig. 6a.

	PLTH
$R_{\rm diskbb}$ (km)	150^{+15}_{-13}
$kT_{\rm th}$ (keV)	27^{+5}_{-4}
$\tau_{\rm th}$	$1.6^{+0.3}_{-0.2}$
$\tau_{\rm pl}$	$0.29^{+0.08}_{-0.07}$
p	$4.5^{+0.3}_{-0.3}$
$\Omega/2\pi$	$1.22^{+0.08}_{-0.13}$
ξ (erg cm s^{-1})	42^{+14}_{-7}
$R_{\rm ref}$ (R_g)	(6)
$E_{\rm line}$ (keV)	$5.60^{+0.06}_{-0.06}$
EW (eV)	220
χ^2/ν	65.9/94

Compton cooling relative to Coulomb cooling, so a larger fraction of the non-thermal electrons thermalize for small $\ell_{\rm s}$. The effects of this can be offset by putting less power into the thermal heating of the electrons i.e. by increasing $\ell_{\rm nth}/\ell_{\rm h}$. A model HYBN (see Table 4) with all the hard power in the non-thermal injection (fixed $\ell_{\rm nth}/\ell_{\rm h}$ = 1, but $\ell_{\rm s}$ left free) is statistically acceptable ($\Delta\chi^2 = +1.7$ compared to model HYB). This model has $\ell_{\rm s} \approx 0.8$, which is a firm lower limit on the soft compactness.

An upper limit on the soft compactness can also be found from the spectrum. Since the hard-to-soft compactness ratio is very well determined by the spectral shape, $\ell_{\rm h}/\ell_{\rm s} \approx 1$, large $\ell_{\rm s}$ requires large $\ell_{\rm h}$. But there is an upper limit on the hard compactness, since large $\ell_{\rm h}$ gives rise to a strong annihilation line which is not present in the data. Thus, we can roughly constrain the soft compactness, $1 \lesssim \ell_{\rm s} \lesssim 20$ and the total compactness, $2 \lesssim \ell \lesssim 40$.

The contribution of electron-positron pairs to the Comptonizing plasma is negligible, as the best-fitting model yields $\tau_{\rm pair} \sim 10^{-3}$. The plasma would be pair-dominated ($\tau_{\rm pair} > \tau_{\rm ion}$) only for extremely high compactness, $\ell \gtrsim 3000$, which is ruled-out by the data ($\chi^2/\nu \sim 128/94$).

The Compton reflection requires a substantial amount of relativistic smearing. We fix the inner disc radius at $R_{\rm ref} = 10R_g$ during the fit, but values higher that $\sim 15R_g$ are ruled-out. The best-fitting model give unphysical rest-frame iron line energy of 5.6 keV. This probably indicates that the Compton reflection model we use here is inadequate, as already inferred from the *ASCA* fits (Section 5.1).

These fits can be dramatically improved ($\chi^2/\nu = 63.4/92$, model HYBTH) by including an additional, optically thick, thermal Comptonization component (for which we use THCOMP code). The residuals in Figs. 6b and 6c show that the improvement affects the whole spectral range, though in particular the features below ~ 10 keV are substantially smoothed. The model is detailed in Table 4, but again the complex correlations between parameters mean that again the errors are only representative as we fixed $\ell_{\rm nth}/\ell_{\rm h}$ = 0.59 (from model HYB) and $R_{\rm ref} = 30R_g$.

The hot plasma properties are insensitive to the presence of the additional thermal Compton component. Both HYB and HYBTH models predict $\ell_{\rm h}/\ell_{\rm s} \approx 1$ and a significant fraction of the hard power from non-thermal electrons ($\ell_{\rm nth}/\ell_{\rm h} \gtrsim 0.5$). They both rule out pair-dominated plasma. The main difference is in the optical depth of the Comptonizing medium, which decreased from $\sim$2.8 to $\sim$1.8 when THCOMP was added.

Table 4. Fitting results with a hybrid thermal/non-thermal model. HYB is the hybrid model with fixed $\ell_{\rm s}$ = 10 and free $\ell_{\rm nth}$. HYBN is the hybrid model with free $\ell_{\rm s}$ and fixed $\ell_{\rm nth}$ = 1 (no thermal heating). HYBTH stands for the hybrid model with additional component with thermal electrons. Values in parentheses refer to the parameters fixed during the fit. The equilibrium temperature, T_e, was calculated self-consistently and was not a fit parameter.

	HYB	HYBN	HYBTH
$R_{\rm diskbb}$ (km)	197^{+7}_{-7}	200^{+6}_{-6}	186^{+10}_{-10}
$kT_{\rm th}$ (keV)	–	–	$7.7^{+0.5}_{-0.6}$
$\tau_{\rm th}$	–	–	$6.4^{+0.8}_{-1.0}$
$\ell_{\rm s}$	(10)	$0.81^{+0.17}_{-0.24}$	(10)
$\ell_{\rm nth}/\ell_{\rm h}$	$0.59^{+0.03}_{-0.04}$	(1.00)	(0.59)
$\ell_{\rm h}/\ell_{\rm s}$	$1.04^{+0.04}_{-0.04}$	$0.90^{+0.04}_{-0.03}$	$0.94^{+0.04}_{-0.03}$
kT_e (keV)	12	20	20
$\tau_{\rm ion}$	$2.78^{+0.07}_{-0.06}$	$1.77^{+0.06}_{-0.15}$	$1.76^{+0.07}_{-0.08}$
$\Gamma_{\rm inj}$	$3.19^{+0.06}_{-0.09}$	$3.22^{+0.07}_{-0.12}$	$3.34^{+0.08}_{-0.08}$
$\Omega/2\pi$	$0.76^{+0.07}_{-0.09}$	$1.17^{+0.05}_{-0.09}$	$0.32^{+0.12}_{-0.04}$
ξ (erg cm s^{-1})	190^{+110}_{-50}	100^{+15}_{-10}	8000^{+17000}_{-6000}
$R_{\rm ref}$ (R_g)	(10)	(10)	(30)
$E_{\rm line}$ (keV)	$5.89^{+0.06}_{-0.06}$	$5.84^{+0.07}_{-0.04}$	$6.23^{+0.07}_{-0.06}$
χ^2/ν	100.6/94	102.3/94	63.4/92

The extrapolated unabsorbed bolometric flux of XTE J1550–564 from both models is 1.1×10^{-7} erg cm^{-2} s^{-1}. At a distance of 5.3 kpc, for a 10M$_\odot$ black hole, this corresponds to about $0.3L_{\rm Edd}$.

6 HIGH AND VERY HIGH X-RAY SPECTRAL STATES

As we have outlined in the introduction, there are at least two distinct soft spectral states of black hole binaries: high and very high. We attribute our observation of XTE J1550–564 to the very high state. How does it compare with other sources, in both soft states? Fig. 7 shows a comparison of the high- and very high-state model spectra. The high-state spectrum is from Cyg X-1 (Gierliński et al. 1999) while the very high-state one is from XTE J1550–564 (this paper). The same model is used for both, with a hybrid electron distribution calculated using the EQPAIR code (Coppi 1999).

The main difference between the high and very high states seems to be the amount of Comptonization of the disc spectrum. In the high state many of the disc photons escape without being strongly Comptonized, therefore the Comptonizing plasma either covers only a small fraction of the disc and/or has low optical depth. In the very high state most of the disc emission is scattered to substantially higher energies, so the Comptonizing medium must have a substantial optical depth and cover most of the disc.

However, we caution that the amount of Comptonization is not always straightforward to derive from the spectra. For example, Zdziarski et al. (2001) fit two soft state *RXTE*/OSSE spectra from GRS 1915+105. The 'ultrasoft' high-state spectrum (VP 813) has a strong, dominating soft component and a weak high-energy tail. It is similar to the Cyg X-1 spectrum from Fig. 7, but the temperature of the soft component and its ratio of power to the hard tail is larger. The second observation analyzed by Zdziarski et al. (2001) is a typical very high-state spectrum (VP 619), with comparable distribution of power between the disc and the tail, similar to the

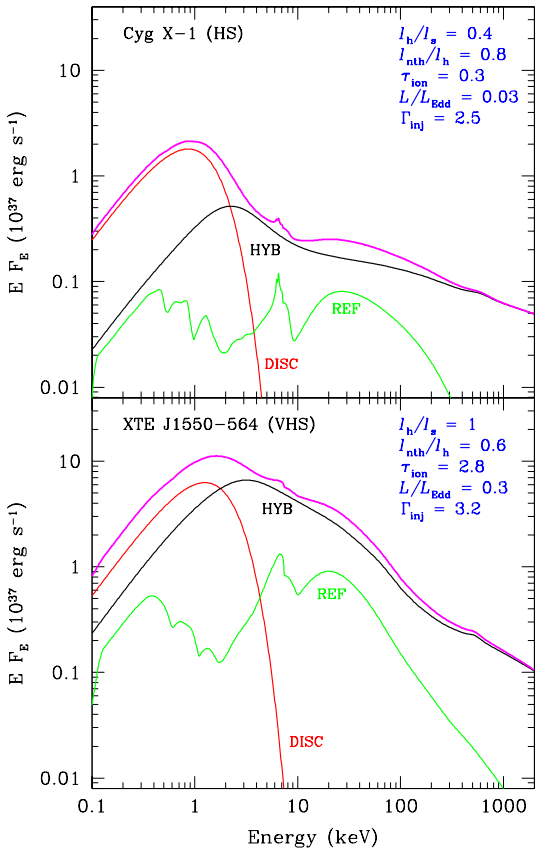

Figure 7. Unabsorbed model components for Cyg X-1 in the high state (from Gierliński et al. 1997) and XTE J1550–564 in the very high state (this paper, model HYB). The approximate values of some of the best-fitting EQPAIR parameters are given. To convert fluxes into luminosities we assumed distances of 2 kpc for Cyg X-1 and 5.3 kpc for XTE J1550–564. For Eddington luminosities we assumed $10 M_\odot$ black hole mass for both sources.

XTE J1550–564 spectrum analysed here (see fig. 2 in Zdziarski et al. 2001). However, the detailed spectral modelling with EQPAIR suggests a rather different interpretation of this high state to that outlined above. What looks like a disc in the high-state spectrum of GRS 1915+105 is fit by Comptonization of the disc in optically thick, low-temperature plasma, very different to the high state of Cyg X-1. However, it seems more likely that this simply reflects the fact that the disc spectral models do not adequately describe the observed disc emission. The dominating soft component in GRS 1915+105 probably comes from the disc itself, while an optically thin, hot plasma is responsible for the weak hard tail. Thus we conclude that there is probably an increase in the covering fraction and/or optical depth of the Comptonizing plasma which drives the source evolution from the high to very high states.

Another difference between the high and very high states is a change in shape of the non-thermal tail. The power-law index of the injected electron distribution is steeper in the very high state than in the high state, as is also seen in GRS 1915+105 (Zdziarski et al. 2001). Thus it seems that there are also changes in the non-thermal electron acceleration associated with the source moving from high to very high state.

7 DISCUSSION AND CONCLUSIONS

During its 1998/1999 outburst the black hole candidate XTE J1550–564 showed a variety of X/γ-ray spectral states. In this paper we have analyzed its broadband spectrum during the very high state. This spectral state is characterised by the presence of the soft, high-energy tail extending without any apparent break above $\sim$ 300 keV. Such a tail differs from the low/hard state tail both in having a significantly softer spectral index and in the lack of high-energy cutoff (Grove et al. 1998). Phenomenologically, the OSSE spectra of these tails can be described as a power law with spectral index $\Gamma \sim 2.4$–3.1 (Grove et al. 1998). In this observation $\Gamma = 3.09 \pm 0.04$. We have shown that the broadband X/γ-ray spectrum of XTE J1550–564 can be well fit by a model in which seed photons from the disc are Compton up-scattered by both thermal and non-thermal electrons. Comptonization on purely thermal or purely power-law electrons can be ruled out.

The thermal and non-thermal electron distributions may be distinct, or they may instead form a single hybrid thermal/non-thermal distribution. This is reflected in the modelling of the XTE J1550–564 spectrum, which we have fitted by separate thermal plus non-thermal (model PLTH) and hybrid (model HYB) Comptonizations. However, even if there is a spatially separate non-thermal electron population, these electrons will interact via Coulomb collisions, creating a thermal low-energy extension to the power-law distribution. Thus, we expect a hybrid distribution of Comptonizing electrons even from a completely non-thermal electron acceleration mechanism. Therefore, the PLTH model seems to be less physically motivated, and a single hybrid plasma (HYB) would be our model of choice as the simplest, physical description of the data. However, spectral fitting gives the opposite result, with the less physical model (PLTH) being strongly statistically preferred.

Since we expect that the non-thermal electrons form a hybrid plasma, the next step in complexity would be two separate electron distributions, with one thermal and one hybrid (rather than one thermal and one power law). This model (HYBTH) provides an excellent fit to the data, statistically similar to PLTH but without using an unphysical power law electron distribution. However, closer examination of the Maxwellian component in HYBTH (component denoted as TH in Fig. 6*c*) reveals its suspicious similarity in spectral shape to the Compton reflected continuum. Perhaps it is not due to emission from some thermal, optically thick plasma at all. Perhaps it simply accounts for inaccuracies of the reflection model. In particular, the reflection model used here overestimates the depth of the iron edge for ionized material as it does not include Compton upscattering (Ross, Fabian & Young 1999). While the single hybrid plasma (HYB) is *statistically* ruled out when compared to the two-component solution (HYBTH), better reflection models are required before this can be a robust conclusion.

Whatever is the physical reality behind this additional thermal Compton component, the properties of the hybrid plasma are established quite robustly and do not change much between HYB and HYBTH. The ratio of soft to hard compactness is very well defined by the shape of the spectrum ($\ell_\mathrm{h}/\ell_\mathrm{s} \approx 1$), while the fraction of the power in non-thermal electrons is $\ell_\mathrm{nth}/\ell_\mathrm{h} \gtrsim 0.5$. Once again, the presence of non-thermal electrons is required to form the high energy tail observed beyond 300 keV. But where do they come from?

One obvious mechanism for such high-energy emission is from a jet, as in the blazars and radio-loud quasars (see e.g. Ghisellini et al. 1998). A jet is present in XTE J1550–564 indeed at this time, although its radio emission is declining rapidly throughout

the OSSE observation (Wu et al. 2002), so its link with the X/γ-ray emission is doubtful. Moreover, the fact that a similar high-energy tail is seen in the high state as well as in the very high state immediately rules out a direct association with the jet as the radio emission is strongly quenched in the high state (Corbel et al. 2000).

An alternative mechanism of bulk motion of in-falling material near the black hole horizon was proposed by Chakrabarty & Titarchuk (1995), but the free fall results in fairly low electron energies, with Lorentz factors $\gamma \lesssim 1.4$. These electrons are unable to up-scatter photons past $\sim$ 100–300 keV, resulting in a cutoff in the power-law spectrum (Laurent & Titarchuk 1999; Zdziarski et al. 2001). Since such a cutoff is not seen in the XTE J1550–564 data, we find the bulk motion Comptonization to be an unlikely explanation of the observed emission.

This leaves magnetic reconnection above the disc as the only known possible source of hard X-ray dissipation at high mass accretion rates. The accretion disc viscosity is now known to be linked to a magnetic dynamo, so magnetic buoyancy can lead to some fraction of the reconnection events occurring in a corona rather than deep inside the disc (see e.g. Hawley & Balbus 2002), accelerating electrons to high energies (di Matteo 1998). We speculate that the high and very high state spectra are continuous rather than two separate spectral states, linked by an increase in the covering fraction of this magnetic corona over the disc.

Concluding our paper we summarise our main results:

- The broad-band X/γ-ray spectrum of XTE J1550–564 in the very high state can be well described by inverse Compton emission from hybrid, thermal/non-thermal plasma.
- Comptonization on purely thermal or purely power-law electrons cannot explain the observed spectrum.
- The high-energy power-law tail observed here is similar in other black hole binaries in the high and very high states, showing that it is a generic property of high mass accretion rate black holes.

ACKNOWLEDGEMENTS

This research has been supported in part by the Polish KBN grant 2P03D00514. We thank John Tomsick for providing the computer code for the PCA pile-up correction and Aya Kubota for useful discussions.

REFERENCES

Arnaud K. A., 1996, in Jacoby G. H., Barnes J., eds., Astronomical Data Analysis Software and Systems V. ASP Conf. Series Vol. 101, San Francisco, p. 17
Bałucińska-Church M., Belloni T., Church M. J., Hasinger G., 1995, A&A, 302, L5
Belloni T., Méndez M., van der Klis M., Hasinger G., Lewin W. H. G., van Paradijs J., 1996, ApJ, 472, L107
Blumenthal G. R., Gould R. J., 1970, Reviews of Modern Physics, 42, 237
Brandt W. N., Schulz N. S., 2000, ApJ, 544, L123
Brocksopp C., et al., 2002, MNRAS, 331, 765
Chakrabarty S., Titarchuk L. G., 1995, ApJ, 455, 623
Chen W., Shrader C. R., Livio M., 1997, ApJ, 491, 312
Coppi P. S., 1999, in ASP Conf. Ser. 161, High Energy Processes in Accreting Black Holes, ed. J. Poutanen & R. Svensson (San Francisco: ASP), 375
Corbel S., Fender R. P., Tzioumis A. K., Nowak M., McIntyre V., Durouchoux P., Sood R., 2000, A&A, 359, 251
Di Matteo T., 1998, MNRAS, 299, L15
Di Salvo T., Done C., Życki P. T., Burderi L., Robba N. R., 2001, ApJ, 547, 1024
Done C., Gierliński M., 2003, MNRAS, submitted (astro-ph/0211206)
Done C., Madejski G. M., Życki P. T., 2000, ApJ, 536, 213
Done C., Życki P. T., Smith D. A., 2002, MNRAS, 331, 453
Ebisawa K., et al. 1994, PASJ, 46, 375
Esin A. A., McClintock J. E., Narayan R., 1997, ApJ, 489, 865
Esin A. A., Lasota J.-P., Hynes R. I., 2000, A&A, 354, 987
Fabian A. C., Rees M. J., Stella L., White N. E., 1989, MNRAS, 238, 729
Frontera F., et al., 2001, ApJ, 561, 1006
Ghisellini G., 1989, MNRAS, 236, 341
Ghisellini G., Celotti A., Fossati G., Maraschi L., Comastri A., 1998, MNRAS, 301, 451
Gierliński M., Done C., 2002, MNRAS, 331, L47
Gierliński M., Zdziarski A. A., Done C., Johnson W. N., Ebisawa K., Ueda Y., Haardt F., Phlips B. F., 1997, MNRAS, 288, 958
Gierliński M., Zdziarski A. A., Poutanen J., Coppi P. S., Ebisawa K., Johnson W. M., 1999, MNRAS, 309, 496
Grove J. E., Johnson W. N., Kroeger R. A., McNaron-Brown K., Skibo J. G., Phlips B. F., 1998, ApJ, 500, 899
Hawley J. F., Balbus S. A., 2002, ApJ, 573, 738
Homan J., Wijnannds R., van der Klis M., Belloni T., van Pradijs J., Klein-Wolt M., Fender R., Méndez M., 2001, ApJSS, 132, 377
Jain R. K., Bailyn C. D., Orosz J. A., Remillard R. A., McClintock J. E., 1999, ApJ, 517, L131
Johnson W. N., et al., 1993, ApJS, 86, 693
Kompaneets A. S., 1956, Soviet Phys., JETP 31, 876
Kong A. K. H., Kuulkers E., Charles P. A., Homer L., 2000, MNRAS, 312, L49
Kong A. K. H., McClintock J. E., Garcia M. R., Murray S. S., Barret D., 2002, ApJ, 570, 277
Kotani T., Ebisawa K., Dotani T., Inoue H., Nagase F., Tanaka Y., Ueda Y., 2000, ApJ, 539, 413
Kubota A., Makishima K., Ebisawa K., 2001, ApJ, 560, L147
Kubota A., et al., 2003, in preparation
Laurent P., Titarchuk L., 1999, ApJ, 511, 289
Magdziarz P., Zdziarski A. A., 1995, MNRAS, 273, 837
Makishima K., et al., 1996, PASJ, 48, 171
McConnell M. L., et al., 2002, ApJ, 572, 984
Méndez M., van der Klis M., 1997, ApJ, 479, 926
Merloni A., Fabian A. C., Ross R. R., 2000, MNRAS, 313, 193
Mitsuda K., et al., 1984, PASJ, 36, 741
Orosz J. A., et al., 2002, ApJ, 568, 845
Ross R. R., Fabian A. C., Young A. J., 1999, MNRAS, 306, 461
Poutanen J., Svensson R., 1996, ApJ, 470, 249
Poutanen J., Krolik J. H., Ryde F., 1997, MNRAS, 292, L21
Rothschild R. E., et al., 1998, ApJ, 496, 538
Shimura T., Takahara F., 1995, ApJ, 445, 780
Smith D. A., et al., 1998, IAU Circ. 7008
Sobczak G. J., McClintock J. E., Remillard R. A., Cui W., Levine A. M., Morgan E. H., Orosz J. A., Bailyn C. D., 2000b, ApJ, 544, 993
Sunyaev R. A., Titarchuk L. G., 1980, A&A, 86, 121
Sutaria F. K., et al., 2002, A&A, 391, 993
Titarchuk L. G., Shrader C. R., 2002, ApJ, 567, 1057
Tomsick J. A., Corbel S., Kaaret P., 2001, ApJ, 563, 229
Tomsick J. A., Kaaret P., Kroeger R. A., Remillard R. A., 1999, ApJ, 512, 892
Ueda Y., Inoue H., Tanaka Y., Ebisawa K., Nagase F., Kotani T., Gehrels N., 1998, ApJ, 492, 782
Ueda Y., et al., 2002, ApJ, 571, 918
Wilson C. D., Done C., 2001, MNRAS 325, 167
Wu K., et al., 2002, ApJ, 565, 1161
Zdziarski A. A., Johnson W. N., Magdziarz P., 1996, MNRAS, 283, 193
Zdziarski A. A., Poutanen J., Mikołajewska J., Gierliński M., Ebisawa K., Johnson W. N., 1998, MNRAS, 301, 435
Zdziarski A. A., Grove J. E., Poutanen J., Rao A. R., Vadawale S. V., 2001, ApJ, 554, L45

Zdziarski A. A., Poutanen J., Paciesas W. S., Wen L., 2002, ApJ, 578, 357
Zhang S. N., Cui W., Chen W., 1997, ApJ, 482, L155
Życki P. T., Done C., Smith D. A., 2001, MNRAS, 326, 1367